# Free-free transitions of the *e*-H system inside a dense plasma irradiated by a laser field at very low incident-electron energies

A. K. Bhatia[1] and C. Sinha[2]

[1]*Solar Physics Laboratory, NASA/Goddard Space Flight Center, Greenbelt, Maryland 20771, USA*

[2]*Theoretical Physics Department, Indian Association for the Cultivation of Science, Jadavpur, Kolkata 700032, India*

(Received 13 June 2012; published 28 November 2012)

The free-free transition is studied for an electron-hydrogen atom in ground state when a low-energy electron (external) is injected into hydrogenic plasma in the presence of an external homogenous, monochromatic, and linearly polarized laser field. The effect of plasma screening is considered in the Debye-Hückel approximation. The calculations are performed in the soft photon limit. The incident electron is considered to be dressed by the laser field in a nonperturbative manner by choosing the Volkov solutions in both the initial and final channels. The space part of the scattering wave function for the electron is solved numerically by taking into account the electron exchange. The laser-assisted differential and total cross sections are calculated for single-photon absorption or emission and no-photon exchange in the soft photon limit, the laser intensity being much less than the atomic field intensity. The calculations have been carried out for various values of Debye parameter, ranging from 0.005 to 0.12. A strong suppression is noted in the laser-assisted cross sections as compared to the field-free situation. A significant difference is noted for the singlet and triplet cross sections. The suppression is much more in the triplet states.

DOI: 10.1103/PhysRevA.86.053421 PACS number(s): 34.80.Qb, 34.50.Rk

## I. INTRODUCTION

In recent years much attention has been paid to the atomic processes of different atomic systems embedded in plasma. The motivations for such studies are manifold and were already emphasized in earlier works [1–10] (see further references cited therein). The purpose of the present work is to study the influence of an external laser field on the free-free transition process of an electron-hydrogen system in a plasma environment. Such studies have direct relevance to many real physical objects, e.g., laser-produced plasma [7], fusion plasma confinement, high-power gas lasers, etc. In particular, the inverse bremsstrahlung process is believed to play an important role in the breakdown and the heating process of plasma illuminated by a laser beam [10]. The interpretation of the line emission from plasma requires a detailed knowledge of the spectroscopic as well as the collisional properties (e.g., collision strength, cross sections, etc.) of the plasma constituents. However, not much is known about the combined effects of plasma and laser field on the important collision processes [7,10]. When plasma is irradiated with an external laser field, there will be a transfer of energy from the laser to the plasma without altering the average plasma properties [11]. Further, a laser field can produce substantial narrowing of the spectral lines emitted from a plasma as well as it can change their shapes (depending on the plasma parameters) by decreasing the Stark broadening [12–14] which is very useful in the plasma diagnosis. This significant decrease in the Stark width of the hydrogenic as well as nonhydrogenic spectral lines in turn increase the gain of lasers, in particular, the x-ray lasers [12], since for any laser, the gain is inversely proportional to the linewidth.

Although a plasma is often thought of as a quasineutral ensemble of electrons and completely stripped nuclei (such as protons), there is of course no such ideal plasma. First of all, 100% ionization is an asymptotic approximation, and second, there continually exist with some orbiting electron ions that exhibit atomic bound state characteristics and undergo atomic processes. Most laboratory plasmas have a beginning as a neutral atomic or molecular gas and they exist in various ionic states for a finite period of time until the ultimate degree of ionization is achieved [15]. Therefore, we can assume that there are neutral hydrogen atoms in the plasma which are surrounded by perturbing particles (electrons and ions). These perturbers produce a screened Coulomb potential.

Inside plasma, partial shielding by the neighboring charged particles weakens the pure Coulomb interaction between two charged particles at large separations, thereby affecting the collision cross sections for an external electron incident on the plasma. It is therefore expected that the effect of plasma screening on the collision cross sections should be particularly large at low incident energies [6].

In most of the collisional experiments with or without the presence of laser field, the plasma environment is always present to some extent and it can significantly affect the collision process. It is therefore desirable and quite worthwhile to study the atomic collision processes under the combined presence of plasma and the laser field. Due to the rapid and dynamic development in laser technology, laser-assisted collision experiments are becoming increasingly feasible at laboratories where a significant number of theoretical studies were performed for different atomic collision processes. Laser-assisted excitation, ionization, recombination, and the free-free transition processes are the basic underlying mechanisms for different highly nonlinear phenomena, e.g., nonsequential double ionization (NSDI) or nonsequential multiple ionization, high-harmonic generation (HHG), and high-order above-threshold ionization (HATI) that occur when atomic or molecular targets are irradiated with strong and short wavelength laser fields. The Coulomb potential of the system is distorted by such fields and as a result, the electron can escape from the atoms (or molecules) through tunneling. If the

 

tunneled electron driven by the laser field revisits its parent atomic ion during the reverse cycle of the laser field, the electron again may either be elastically scattered from its parent ion leading to HATI peaks or it can recombine with it generating a high-order harmonic (HHG). The tunneled electron can also reionize the residual nucleus leading to NSDI. It is therefore expected that the laser-assisted collisional experiments where the collision partners are under full control could provide detailed insight into the above phenomena.

Apart from these, the laser-assisted electron-atom collision allows, on the one hand, the experimental observation of different multiphoton processes [16–20] at relatively moderate laser field intensities, while on the other hand, it allows one to measure some electron-atom scattering parameters which otherwise would not be accessible to experiments. In view of the recent availability of the tunable lasers with a wide frequency range, unique effects can be observed which are not present in ordinary electron-atom scattering.

In a recent work [21], we investigated the effect of an external laser field on the scattering of low-energy electrons from the ground-state hydrogen atoms in a gaseous medium. Wallbank and Holmes [19] carried out experiments on the scattering of low-energy electrons from He atoms in the presence of a pulsed $CO_2$ laser with the laser polarization parallel to the momentum transfer and the photon energy being 0.117 eV. Our results for the H atom [21] were found to be in accord with the experiment [19] qualitatively.

The present work addresses the laser-assisted free-free (FF) transition of a plasma-embedded electron-hydrogen (ground-state) system at very low incident energies in the framework of the Debye-Hückel model [22]. It should be pointed out that the low-energy incident electron is an external electron and not the plasma electron. The present work is concerned only with the role of the plasma as the static screening (Debye) potential [22]. However, it should be mentioned that in general, apart from this screening effect, the plasma can also interact with the atoms providing an extra broadening or narrowing of levels of the hydrogen atoms as well as it can interact with the incident beam of electrons and the laser field. Regarding the plasma-atom interaction, the present assumption is supposed to be quite safe since the ground state of the atom, considered here, is hardly affected by this. It should also be emphasized that beam penetration is not expected to be affected because the low-energy incident electron will undergo elastic scattering due to the screened Coulomb potential. Furthermore, no instabilities should be introduced in the plasma because the incident electron is not able to excite the higher states of the atoms and ions.

## II. THEORY

The free-free transition in the presence of an external laser field is given by

$$\omega(l) + e^-(\vec{k}_i) + H(1s) \rightarrow e^-(\vec{k}_f) + H(1s), \tag{1}$$

where $l$ is the number of photons absorbed or emitted. The processes in which $l < 0$ and $l > 0$ correspond to stimulated bremsstrahlung (emission) and inverse bremsstrahlung (absorption), respectively, while $l = 0$ corresponds to pure laser-assisted elastic (free-free) scattering; $\vec{k}_i$ and $\vec{k}_f$ are the incident and final momenta of the projectile electron.

The laser field is chosen to be homogeneous, monochromatic, and linearly polarized and is represented by $\vec{\varepsilon}(t) = \vec{\varepsilon}_0 \sin(\omega t + \xi)$, where $\xi$ is the initial phase of the laser field, the corresponding vector potential in the dipole approximation is $\vec{A}(t) = \vec{A}_0 \cos(\omega t + \xi)$ with $\vec{A}_0 = c\vec{\varepsilon}_0/\omega$, and $\xi$ is chosen equal to zero in the present work. The laser field $\vec{\varepsilon}$ corresponds to laser polarization, parallel to the incident electron momentum.

The total Hamiltonian of the system in the laser field is given by

$$H = -(i\vec{\nabla}_1 + \vec{A})^2 - (i\vec{\nabla}_2 + \vec{A})^2 + V_D, \tag{2}$$

where $V_D$ represents the Debye-Hückel potential [22] of the form

$$V_D = -\frac{2Z}{r_1}e^{-\mu r_1} - \frac{2Z}{r_2}e^{-\mu r_2} + \frac{2}{r_{12}}e^{-\mu r_{12}}, \tag{3}$$

where $\vec{r}_1$ and $\vec{r}_2$ are the position vectors of the incident electron and the bound electron of the target hydrogen atom, and $r_{12}$ is the relative distance. The parameter $\mu$ is called the Debye screening parameter and is given by $\mu = [4\pi n(Ze)^2/k_B T]^{0.5} = 1/D$, where $k_B$ is the Boltzmann constant, $n$ is the plasma density, and $T$ is the temperature of the plasma. The Debye length is given by $1/\mu = D$. We use Rydberg units throughout our calculations. Therefore, $\mu$ has the units of $1/a_0$, where $a_0$ is the Bohr radius of the hydrogen atom. We have carried out calculations for $\mu = 0.005$ to 0.12, which is a very reasonable choice to study the effects on the scattering process in the presence of the Debye shielding [22].

The energy of the laser field is $\omega = 0.0043$ a.u. $= 0.117$ eV (1 a.u. of energy being 219 474.62 $\text{cm}^{-1}$), i.e., we are dealing with soft photons and the strength of the laser field is $\mathcal{E}_0 = 0.01$ a.u. (1 a.u. being $5 \times 10^9$ V/cm). The incident energy ${k_i}^2$ of the electron ranges from 0.01 to 0.64 Ry or from 0.136 to 8.707 eV in our calculation. This incident energy is very much below the $n = 2$ threshold of the hydrogen atom.

The energy conservation relation for this FF process is given by

$$k_f^2 = k_i^2 + 2l\omega, \quad l = 0, \pm 1, \pm 2, \ldots. \tag{4}$$

The transition matrix element for the laser-assisted process (1) is given by [21]

$$T_{if} = -i \int dt \langle \psi_f | V_f | \Psi_i^+ \rangle, \tag{5}$$

where the perturbation

$$V_f = \left( \frac{2Z}{r_1}e^{-\mu r_1} - \frac{2}{r_{12}}e^{-\mu r_{12}} \right). \tag{6}$$

The projectile electron is considered to be dressed by the laser field in a nonperturbative manner by choosing the Volkov solutions [23] in both the initial and final channels. The final channel asymptotic wave function $\psi_f$ in Eq. (5) satisfies the following Schrödinger equation:

$$\left[ -(i\vec{\nabla}_1 + \vec{A})^2 - (i\vec{\nabla}_2)^2 - \frac{2Z}{r_2}e^{-\mu r_2} - E \right] \psi_f = 0. \tag{7}$$

In the present work, we have neglected the laser-target interactions as compared to the dominant projectile-target interactions at very low incident energies. Thus the final channel wave function $\psi_f$ is chosen as

$$\psi_f = \chi_{k_f}\phi_f. \tag{8}$$

The final-state wave function $\phi_f$ is the same as the initial-state wave function $\phi_0$ given in Eq. (24) and calculated in the presence of the Debye-Hückel [22] potential. The time-dependent Schrödinger equation describing the wave function $\chi_k$ of the electron in the laser field in the Coulomb gauge is given by

$$i\frac{\partial \chi_k^C(\vec{r},t)}{\partial t} = [-\nabla^2 + H(t)]\chi_k^C(\vec{r},t). \tag{9}$$

The superscript "$C$" on the wave function $\chi^C(\vec{r},t)$ indicates the Coulomb gauge and

$$H(t) = i\frac{2q}{c}\vec{A}(t)\cdot\vec{\nabla} + \frac{q^2}{c^2}A^2(t). \tag{10}$$

In the above equation, $q = -e$ is the charge on the projectile. The second term of Eq. (10) can be eliminated by a canonical transformation. The solution of Eq. (9) is then given by the Volkov wave function [23–25]

$$\chi_k^C(\vec{r},t) = (2\pi)^{-3/2}\exp(i\vec{k}\cdot\vec{r} - i[E_k t - \vec{\alpha}_0\cdot\vec{k}\sin(\omega t - \delta)]), \tag{11}$$

where $E_k = k^2$ is the free energy and

$$\vec{A}(t) = \vec{A}_0\cos(\omega t - \delta), \quad \vec{\alpha}_0 = \vec{\varepsilon}_0/\omega^2. \tag{12}$$

Now, we use the generating function of the Bessel functions [26]:

$$\exp(-ik_i\alpha_0\sin\omega t) = \sum_{m=-\infty}^{\infty}(-1)^m\exp(im\omega t)J_m(k_i\alpha_0). \tag{13}$$

Using the above generating function, where $J_m$ is the Bessel function of order $m$, and in view of the relation

$$J_{-m}(z) = (-1)^m J_m(z), \tag{14}$$

Eq. (11) can be recast as (the superscript being omitted)

$$\chi_{k_i}(r,t) = (2\pi)^{-3/2}\sum(-i)^m J_m(k_i\alpha_0) \times \exp\{i[\vec{k}\cdot\vec{r} - (E_{k_i} - m\omega)t]\}. \tag{15}$$

We have chosen $\delta$ equal to zero in Eq. (15). The full scattering wave function $\Psi_i^+$ in the initial channel satisfies the three-body Schrödinger equation, obeying the incoming wave boundary condition:

$$(H - E)\Psi_i^+ = 0. \tag{16}$$

Now the spatial part $\Psi_s(\vec{r}_1,\vec{r}_2)$ of the full scattering wave function $\Psi_i^+$ is obtained numerically in the framework of the partial wave expansion by solving the initial channel Schrödinger equation, incorporating the electron exchange [27]. Finally, $T_{if}$ reduces to

$$T_{if} = \frac{-i}{(2\pi)^{1/2}}\sum\delta\left(E_{k_f} - E_{k_i} + l\omega\right)J_l(\vec{q}\cdot\vec{\alpha}_0)I, \tag{17}$$

where $\vec{q} = \vec{k}_f - \vec{k}_i$ is the momentum transfer, as indicated earlier $l$ is the number of photons absorbed or emitted, and $I$ is the space part of the transition matrix element and is given by

$$I = \iint d^3r_1\, d^3r_2\, \exp(i\vec{k}_f\cdot\vec{r}_1)\varphi_0(\vec{r}_2)V_f(\vec{r}_1,\vec{r}_2)\Psi_i^+(\vec{r}_1,\vec{r}_2). \tag{18}$$

In the weak field limit (i.e., neglecting the target dressing effect), the laser-assisted differential cross section (DCS) for the elastic scattering, for $l$ photons, can be related to the FF differential cross section by the relation [21,23–25]

$$[d\sigma^l(k_i,k_f(l))/d\Omega]_{\text{laser}} = [k_f(l)/k_i]J_l^2(\mathbf{q}\cdot\boldsymbol{\alpha}_0)[d\sigma^l/d\Omega]_{\text{FF}}, \tag{19}$$

where $[\mathrm{d}\sigma^l/\mathrm{d}\Omega]_{\text{FF}}$ is the field-free elastic cross section, $J_l$ are the Bessel functions of integer order $l$, $\vec{q} = \vec{k}_f - \vec{k}_i$ is the momentum transfer, and $\boldsymbol{k}_i$,$\boldsymbol{k}_f$ are the initial and final momenta of the electron.

The above relation, given in Eq. (19), is called the Kroll-Watson [23] approximation. In order to calculate the FF elastic differential and total cross sections, we carry out the calculation of phase shifts in the exchange approximation [27].

The wave function $\Psi_s(\vec{r}_1,\vec{r}_2)$ for the scattering in the exchange approximation [27] is given by

$$\Psi_s(\vec{r}_1,\vec{r}_2) = u(\vec{r}_1)\phi_0(\vec{r}_2) \pm (1 \leftrightarrow 2), \tag{20}$$

where

$$u(\vec{r}) = \frac{u(r)}{r}Y_{L0}(\Omega). \tag{21}$$

The upper sign $(+)$ refers to singlet states and the lower sign $(-)$ to triplet states. The ground-state wave function of the target is given by $\phi_0$ (vide Appendix). The equation for the scattering function $u(r)$ is obtained from

$$\langle\phi_0(\vec{r}_2)|H' - E|\Psi_S(\vec{r}_1,\vec{r}_2)\rangle = 0. \tag{22}$$

The Hamiltonian in the above equation is given by

$$H' = -\nabla_1^2 - \nabla_2^2 + V_D. \tag{23}$$

Carrying out the integration leads to the scattering equation for $u(r)$; by letting $r_1 = r$, we obtain

$$\left[\frac{d^2}{dr^2} - \frac{L(L+1)}{r^2} + \frac{2Z}{r}e^{-pr} - V_3(r) + k^2\right]u(r) \pm\left\{r\varphi_0(r)\delta_{L0}F_1 - \frac{2}{(2L+1)}\varphi_0(r) \times\left[\frac{e^{-\mu r}}{r^L}F(r) + r^{L+1}e^{\mu r}G(r)\right]\right\} = 0, \tag{24}$$

where

$$F_1 = \int_0^\alpha dx\, B(x)u(x), \tag{25}$$

$$F(r) = \int_0^r dx\, x^{(L+1)}e^{-\mu x}\varphi_0(x)u(x), \tag{26}$$

$$G(r) = \int_r^\alpha dx\frac{e^{-\mu x}}{x^L}\varphi_0(x)u(x), \tag{27}$$

$$B(x) = \sum_j C_j [j(j-1)x^{j-2} - 2ajx^{j-1}] + 2Ze^{-\mu x}\phi_0(x) + (k^2+a^2)x\phi_0(x), \quad (28)$$

$$V_3(r) = 2\sum_j C_j \sum_i C_i \left[ \frac{e^{-\mu r}}{r} \left\{ \frac{(j+i)!}{q^{j+i+1}} - e^{-qr} v(r,q) \right\} + e^{\mu r} e^{-pr} w(r,t) \right], \quad (29)$$

where $q = 2a - \mu$ and $p = 2a + \mu$.

$$v(r,q) = \sum_s^{i+j} \frac{(i+j)!}{(i+j-s)!} \frac{r^{i+j-s}}{q^{1+s}} \quad (30)$$

and

$$w(r,p) = \sum_s^{i+j-1} \frac{(i+j-1)!}{(i+j-1-s)!} \frac{r^{i+j-1-s}}{p^{1+s}}. \quad (31)$$

In Eqs. (25) and (27), the upper limit is infinity, in Eqs. (28) and (29) the summation limits are from 0 to $N$, and the minimum value of $s = 0$ in Eqs. (30) and (31). Because of the parameter $\mu$, the resulting integrodifferential equation is quite different from the well-known exchange approximation equation [27]. However, when we put $\mu = 0$, $a = Z = 1$, and $N = 1$ in the above equations, we recover the equation given in [27] for the exchange approximation.

We have solved the resulting equation for $L = 0$ to 7, numerically by the noniterative method [28]. The phase shifts obtained have variational lower bounds and they are calculated from the function $u(r)$,

$$u(r) = A \sin\left(kr - \frac{L\pi}{2} + \eta\right) \quad \text{for} \quad r \to \infty. \quad (32)$$

A better approximation for higher partial waves would have been the use of the method of polarized orbitals [29]. Since the ground-state wave function is rather complicated, the polarized orbital function $u_{1s\to p}$ [29] has to be obtained numerically for each partial wave $L$. This would have made the problem quite cumbersome to solve. Moreover, the long-range polarization potential arises from the expansion of $1/r_{12}$. Since the parameter $\mu$ occurs in the exponential of the term $\exp(-\mu r_{12})/r_{12}$, this term will not contribute when $r_1$ or $r_2$ goes to infinity in the expansion of $1/r_{12}$. This shows that there will not be any long-range potential in this problem. Similarly, the calculations that include correlations [30] would be too much involved. At present, our main interest is to study the behavior of the elastic scattering (free-free) cross sections in the combined effect of the laser field and the Debye-Hückel potential. As indicated above, we assume that beam penetration is not affected and the incident beam does not produce any instabilities in the plasma.

The phase shifts, for singlet and triplet states have been calculated for the partial waves ($L = 0$ to 7) for the values of $\mu$ given in Table I. The FF elastic DCS is given by [21]

$$[d\sigma^l/d\Omega]_{\rm FF} = \left(1/k_i^2\right) \left| \sum (2L+1) \exp[i\delta_L] \times \sin(\delta_L) P_L(\cos\theta) \right|^2, \quad (33)$$

where $\theta$ is the scattering angle between $r$ and the $Z$ axis.

TABLE I. Ground-state energy of the hydrogen atom for various values of $\mu$ with 15 terms in the expansion of the wave function (20).

| Debye parameter $\mu$ | $E_0$ (Ry) |
|---|---|
| 0.0 | −1.00 |
| 0.005 | −9.90[−1] |
| 0.01 | −9.80[−1] |
| 0.015 | −9.70[−1] |
| 0.02 | −9.61[−1] |
| 0.04 | −9.22[−1] |
| 0.08 | −8.49[−1] |
| 0.12 | −7.80[−1] |
| 0.92 | −4.20[−2] |
| 1.14 | −5.50[−3] |
| 1.1473 | −5.34[−6] |
| 1.1474 | +1.86[−6] |

## III. RESULTS AND DISCUSSIONS

We have computed the laser-assisted (LA) free-free transitions (both differential and total) cross sections for the scattering of an incident electron from a hydrogen atom embedded in plasma and as such the incident electron feels the Debye-Hückel potential [22]. Tables II and III demonstrate the present LA total cross sections (TCS) in free-free transition for the incident $k = 0.1$, 0.2, 0.3, 0.5, and 0.8 in both the triplet and singlet states for various values of the parameter $\mu$ along with the corresponding FF cross sections.

We also provide the results obtained by us [21] in the absence of the Debye-Hückel potential. We note that the cross sections change significantly when the irradiated system is embedded in the Debye plasma. As $\mu$ increases from the zero value, the cross section increases remarkably in all the cases ($l = -1,0,1$) up to $\mu = 0.02$, while beyond that they start to decrease.

It should be noted that in all cases, the cross sections are much higher than those obtained in the absence of the Debye potential. This is due to the size of the atom becoming larger as $\mu$ increases. The wave function of the atom is drawn out and the radius of the atom becomes larger than the Bohr radius. It is, therefore, expected that the cross sections would also increase correspondingly. As $\mu$ increases further, the potential $V_D$ becomes weak and the cross section starts decreasing. This fact can be seen from the results for the cross sections given in tables. As noted in [21], here also in all cases the cross sections are very much suppressed as compared to the FF values in the presence of the Debye-Hückel potential.

The previous results obtained in [21] for $\mu = 0$ have been given to show how they are expected to change when only the exchange approximation is used, as in the present calculation. Since the present scattering calculations are not

TABLE II. Comparison of the triplet cross sections with FF cross sections for electron-hydrogen scattering for various values of $\mu$.

| Parameter $\mu$ | $k_i$ | $l=-1$ | $l=0$ | $l=1$ | Field free |
|---|---|---|---|---|---|
| 0.00[a] | 0.1 | 1.14[−1] | 8.21[−1] | 1.15 | 5.15[+1] |
| | 0.2 | 1.72[−1] | 3.51[−1] | 4.32[−1] | 5.52[+1] |
| | 0.3 | 1.35[−1] | 2.40[−1] | 2.60[−1] | 5.49[+1] |
| | 0.5 | 1.55[−1] | 3.29[−1] | 3.19[−1] | 4.87[+1] |
| | 0.8 | 1.51[−1] | 3.42[−1] | 3.24[−1] | 3.07[+1] |
| 0.00 | 0.1 | 1.55[−1] | 1.41 | 1.77 | 6.79[+1] |
| | 0.2 | 2.36[−1] | 6.35[−1] | 7.26[−1] | 6.28[+1] |
| | 0.3 | 1.71[−1] | 3.50[−1] | 3.79[−1] | 5.64[+1] |
| | 0.5 | 1.09[−1] | 1.99[−1] | 2.00[−1] | 4.30[+1] |
| | 0.8 | 8.14[−2] | 1.58[−1] | 1.54[−1] | 2.55[+1] |
| 0.005 | 0.1 | 4.75 | 4.77[+2] | 2.75[+1] | 1.14[+3] |
| | 0.2 | 2.55 | 4.37[+1] | 8.65 | 2.13[+2] |
| | 0.3 | 1.40 | 9.57 | 4.42 | 9.81[+1] |
| | 0.5 | 3.06[−1] | 1.08 | 7.81[−1] | 4.81[+1] |
| | 0.8 | 6.71[−2] | 1.31[−1] | 1.22[−1] | 2.50[+1] |
| 0.01 | 0.1 | 8.51 | 8.45[+2] | 5.29[+1] | 2.08[+3] |
| | 0.2 | 5.31 | 9.35[+1] | 1.85[+1] | 3.92[+2] |
| | 0.3 | 3.03 | 2.18[+1] | 9.77 | 1.54[+2] |
| | 0.5 | 6.69[−1] | 2.66 | 1.86 | 5.79[+1] |
| | 0.8 | 9.96[−2] | 2.68[−1] | 2.29[−1] | 2.59[+1] |
| 0.015 | 0.1 | 9.82 | 9.37[+2] | 6.84[+1] | 2.48[+3] |
| | 0.2 | 7.32 | 1.27[+2] | 2.65[+1] | 5.22[+2] |
| | 0.3 | 4.42 | 3.19[+1] | 1.45[+1] | 2.03[+2] |
| | 0.5 | 1.04 | 4.28 | 2.96 | 6.80[+1] |
| | 0.8 | 1.48[−1] | 4.58[−1] | 3.84[−1] | 2.74[+1] |
| 0.02 | 0.1 | 9.86 | 8.89[+2] | 7.84[+1] | 2.58[+3] |
| | 0.2 | 8.63 | 1.45[+2] | 3.25[+1] | 6.08[+2] |
| | 0.3 | 5.49 | 3.96[+1] | 1.82[+1] | 2.42[+2] |
| | 0.5 | 1.39 | 5.76 | 4.00 | 7.74[+1] |
| | 0.8 | 2.02[−1] | 6.66[−1] | 5.54[−1] | 2.90[+1] |
| 0.04 | 0.1 | 7.33 | 4.89[+2] | 9.23[+1] | 2.17[+3] |
| | 0.2 | 9.88 | 1.44[+2] | 4.28[+1] | 7.11[+2] |
| | 0.3 | 7.46 | 5.15[+1] | 2.59[+1] | 3.23[+2] |
| | 0.5 | 2.39 | 9.80 | 7.00 | 1.06[+2] |
| | 0.8 | 4.16[−1] | 1.46 | 1.22 | 3.53[+1] |
| 0.08 | 0.1 | 3.99 | 1.51[+2] | 7.13[+1] | 1.33[+3] |
| | 0.2 | 7.36 | 7.89[+1] | 3.72[+1] | 6.04[+2] |
| | 0.3 | 6.56 | 4.02[+1] | 2.41[+1] | 3.28[+2] |
| | 0.5 | 3.03 | 1.20[+1] | 8.89 | 1.28[+2] |
| | 0.8 | 7.10[−1] | 2.49 | 2.10 | 4.39[+1] |
| 0.12 | 0.1 | 2.52 | 6.59[+1] | 4.69[+1] | 8.96[+2] |
| | 0.2 | 5.10 | 4.22[+1] | 2.69[+1] | 4.82[+2] |
| | 0.3 | 4.98 | 2.72[+1] | 1.87[+1] | 2.95[+2] |
| | 0.5 | 2.82 | 1.07[+1] | 8.23 | 1.30[+2] |
| | 0.8 | 1.71 | 5.50 | 4.80 | 1.18[+2] |

[a]Results obtained without the Debye potential and using very accurate phase shifts, which include the contribution of short- and long-range correlations.

TABLE III. Comparison of the singlet cross sections with FF cross sections for electron-hydrogen scattering for various values of $\mu$.

| Parameter $\mu$ | $k_i$ | $l=-1$ | $l=0$ | $l=1$ | Field free |
|---|---|---|---|---|---|
| 0.00[a] | 0.1 | 8.81[−1] | 7.85 | 1.01[+1] | 3.87[+2] |
| | 0.2 | 9.68[−1] | 2.90 | 3.10 | 2.43[+2] |
| | 0.3 | 5.03[−1] | 1.13 | 1.21 | 1.38[+2] |
| | 0.5 | 1.30[−1] | 2.59[−1] | 2.55[−1] | 4.15[+1] |
| | 0.8 | 3.35[−2] | 7.79[−2] | 7.25[−2] | 1.04[+1] |
| 0.00 | 0.1 | 1.33 | 1.26[+1] | 1.56[+1] | 5.79[+2] |
| | 0.2 | 1.18 | 3.43 | 3.88 | 2.87[+2] |
| | 0.3 | 5.12[−1] | 1.15 | 1.24 | 1.39[+2] |
| | 0.5 | 9.48[−2] | 1.69[−1] | 1.70[−1] | 3.77[+1] |
| | 0.8 | 9.29[−3] | 1.40[−2] | 1.39[−2] | 8.02 |
| 0.005 | 0.1 | 6.21 | 5.11[+2] | 4.36[+1] | 1.73[+3] |
| | 0.2 | 3.30 | 4.35[+1] | 1.09[+1] | 4.26[+2] |
| | 0.3 | 1.45 | 8.50 | 4.11 | 1.72[+2] |
| | 0.5 | 2.68[−1] | 9.57[−1] | 6.74[−1] | 4.26[+1] |
| | 0.8 | 4.38[−2] | 1.43[−1] | 1.20[−1] | 9.18 |
| 0.01 | 0.1 | 9.88 | 8.62[+2] | 7.15[+1] | 2.65[+3] |
| | 0.2 | 5.78 | 8.92[+1] | 1.94[+1] | 5.88[+2] |
| | 0.3 | 2.84 | 1.92[+1] | 8.46 | 2.19[+2] |
| | 0.5 | 6.09[−1] | 2.47 | 1.68 | 5.21[+1] |
| | 0.8 | 1.12[−1] | 3.93[−1] | 3.29[−1] | 1.15[+1] |
| 0.015 | 0.1 | 1.11[+1] | 9.39[+2] | 8.74[+1] | 3.01[+3] |
| | 0.2 | 7.51 | 1.19[+2] | 2.60[+1] | 7.01[+2] |
| | 0.3 | 4.02 | 2.81[+1] | 1.23[+1] | 2.60[+2] |
| | 0.5 | 9.61[−1] | 4.28 | 2.72 | 6.19[+1] |
| | 0.8 | 1.89[−1] | 6.72[−1] | 5.62[−1] | 1.40[+1] |
| 0.02 | 0.1 | 1.10[+1] | 8.79[+2] | 9.62[+1] | 3.08[+3] |
| | 0.2 | 8.56 | 1.34[+2] | 3.06[+1] | 7.71[+2] |
| | 0.3 | 4.91 | 3.47[+1] | 1.53[+1] | 2.91[+2] |
| | 0.5 | 1.29 | 5.41 | 3.69 | 7.09[+1] |
| | 0.8 | 2.66[−1] | 9.52[−1] | 7.97[−1] | 1.66[+1] |
| 0.04 | 0.1 | 8.10 | 4.54[+2] | 9.95[+1] | 2.16[+3] |
| | 0.2 | 8.94 | 1.25[+2] | 3.59[+1] | 8.12[+2] |
| | 0.3 | 6.36 | 4.40[+1] | 2.10[+1] | 3.45[+2] |
| | 0.5 | 2.21 | 9.27 | 6.46 | 9.69[+1] |
| | 0.8 | 5.48[−1] | 1.95 | 1.64 | 2.60[+1] |
| 0.08 | 0.1 | 1.85 | 9.84[+1] | 3.00[+1] | 5.88[+2] |
| | 0.2 | 5.23 | 5.71[+1] | 2.33[+1] | 5.81[+2] |
| | 0.3 | 5.14 | 3.27[+1] | 1.81[+1] | 3.10[+2] |
| | 0.5 | 2.73 | 1.11[+1] | 8.06 | 1.13[+2] |
| | 0.8 | 8.99[−1] | 3.13 | 2.67 | 3.83[+1] |
| 0.12 | 0.1 | 1.77 | 5.55[+1] | 3.58[+1] | 5.96[+2] |
| | 0.2 | 2.52 | 4.23[+1] | 1.23[+1] | 3.02[+2] |
| | 0.3 | 3.38 | 1.97[+1] | 1.24[+1] | 2.39[+2] |
| | 0.5 | 2.48 | 9.70 | 7.31 | 1.09[+2] |
| | 0.8 | 1.03 | 3.52 | 3.02 | 4.39[+1] |

[a]Results obtained without the Debye-Hückel potential and using very accurate phase shifts, which include the contribution of short- and long-range correlations.

as sophisticated as the previous ones [21], we do not intend to judge the accuracy of the results by comparison with the previous results [21]. However, if we include one more partial wave in the scattering calculation, we find that most cross sections are accurate within 10%–20%. Therefore, we take the overall accuracy of the results in Tables II and III around 30%. This kind of accuracy indicates the need for a better treatment of the scattering problem, which is outside the scope of the present work. Our interest in this work is to see the overall effects of the Debye-Hückel potential in the presence of a laser field.

We note from the tables that as $\mu$ increases from zero, the cross sections initially increase up to a certain value of $\mu$, and beyond that ($\sim\mu = 0.02$) they decrease. This has been explained above due to the target becoming larger in size

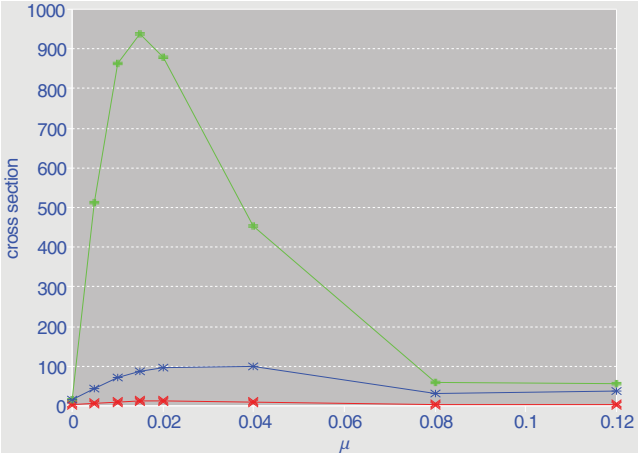


FIG. 1. (Color online) Total cross sections (TCS) vs $\mu = 1/D$ in a.u. for singlet state $k_i = 0.1$. The upper curve is for ($l = 0$), the middle curve is for single-photon absorption ($l = 1$), and the lowest one is for emission ($l = -1$).

as $\mu$ increases from its zero value and then the potential becoming very weak, decreasing the total cross sections. The laser-assisted cross sections are suppressed as compared to the FF ones and the suppression is more for the triplet cross sections than for the singlet ones.

The behavior of the singlet and triplet cross sections, whether LA or FF, is found to be the same as in [21]: the triplet cross sections are lower than the singlet cross sections. This can be explained by noting that the total wave function in the singlet case is space symmetric and therefore the probability of the incident electron to be near the nucleus is much higher than in the triplet case where the wave function is space antisymmetric.

Figures 1–5 exhibit the effect of the laser field on the field-free plasma-embedded cross sections. Figure 1 displays the LA singlet TCS for the cases of single-photon emission ($l = -1$), no-photon transfer ($l = 0$), and single-photon absorption ($l = 1$) with an incident electron momentum $k_i = 0.1$. As may be noted, the cross section has a prominent peak around $\mu = 0.02$, the peak value being dependent on the value of $l$, the photon

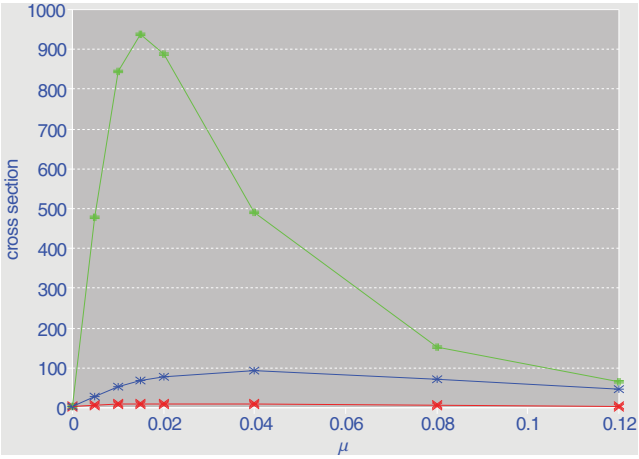


FIG. 2. (Color online) Same as in Fig. 1 but for the triplet case.

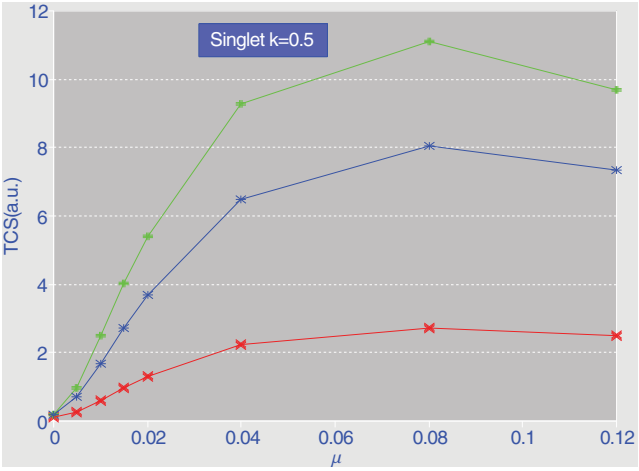


FIG. 3. (Color online) TCS vs $\mu = 1/D$ in a.u. for singlet state $k_i = 0.5$. The upper curve is for ($l = 0$), the middle curve is for single-photon absorption ($l = 1$), and the lowest one is for emission ($l = -1$).

number exchanged. Cross sections decrease very rapidly as $\mu$ increases up to a value ~0.08 beyond which the TCS becomes almost independent of $\mu$. For low incident energies ($k_i = 0.1$), the peak of the TCS occurs at a much lower value of $\mu$, i.e., for a larger value of the Debye length, indicating that the projectile electron is moving in an almost pure Coulombic potential. In Fig. 2 the same qualitative behavior is noted for the triplet case. Figure 2 reveals the same behavior as is observed in the triplet case for $k = 0.1$.

Figure 3 reveals the effect of the laser field and the Debye-Hückel potential on the TCS for a single-photon emission ($l = -1$), no-photon transfer ($l = 0$), and a single-photon absorption ($l = 1$) with an incident $k = 0.5$ in the singlet state. The cross section (TCS) is found to rise gradually and have peaks at around $\mu =\sim 0.08$, beyond which it falls off very slowly and becomes almost constant for higher values of $\mu$. The cross sections are smaller in magnitude as compared

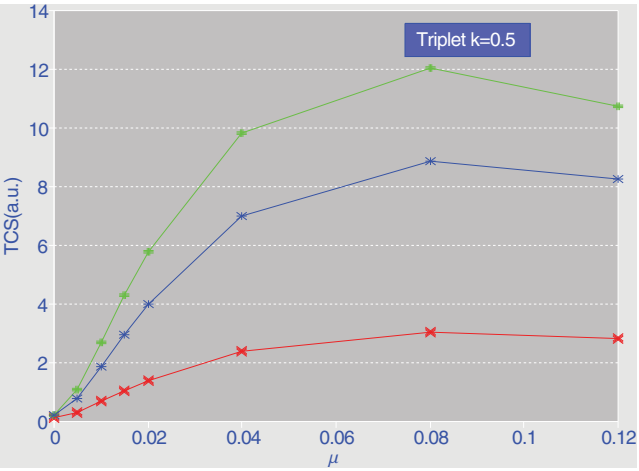


FIG. 4. (Color online) Total cross sections (TCS) vs $\mu = 1/D$ in a.u. for triplet state $k_i = 0.5$. The upper curve is for ($l = 0$), the middle curve is for single-photon absorption ($l = 1$), and the lowest one is for emission ($l = -1$).

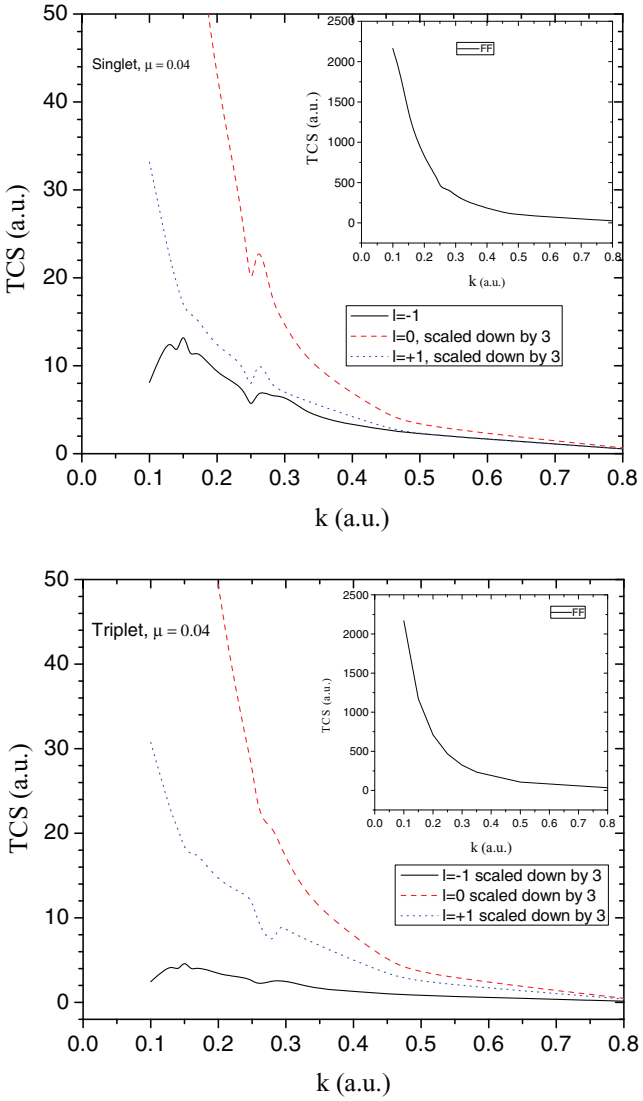


FIG. 5. (Color online) Total singlet (a) and triplet (b) cross sections (TCS) in a.u. against momentum $k_i$ (a.u.). The upper curve is for no-photon exchange ($l = 0$), the middle curve is for single-photon absorption ($l = +1$), and the lowest is for the emission ($l = -1$).

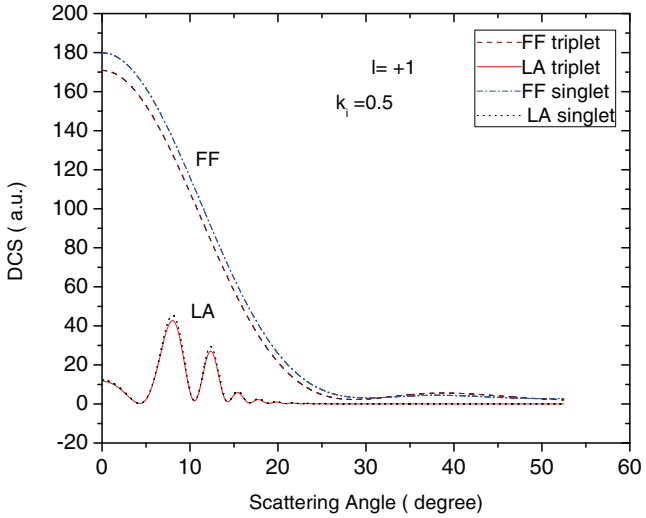


FIG. 6. (Color online) Singlet and triplet DCS for the parameters $k_i = 0.5$, $\mu = 0.02$, and $l = +1$ along with the corresponding FF DCS.

to those for $k_i = 0.1$ as expected. The peak value of the TCS occurs at a much higher value of $\mu$ (compare Figs. 1 and 3), i.e., at a lower Debye length for higher incident energy indicating that the Debye screening increases with increasing incident energy since in this case the incident electron moves closer to the target. Figure 4 exhibits a similar behavior for the triplet state for $k_i = 0.5$ as noted for the singlet one (vide Fig. 3).

Figures 5(a) and 5(b) exhibit a comparative study of the different laser-assisted TCS ($l = 0, \pm 1$) against the incident energy $k$ for both the singlet [Fig. 5(a)] and triplet states [Fig. 5(b)] at $\mu = 0.04$. As may be noted from the Tables I and II, as well as from Fig. 6, the laser-assisted TCS (for $l = 0, \pm 1$) are highly suppressed with respect to the FF (5–6 times) for all values of $\mu$, the suppression being increased with increasing incident energy for higher $\mu$ (e.g., $\mu = 0.04$), while for lower $\mu$, the reverse is true, i.e., the degree of suppression with respect to the FF decreases with increasing incident energy. On the contrary, the difference between the single-photon absorption or emission ($l = \pm 1$) and the no-photon exchange ($l = 0$) TCS decreases with increasing incident energy. The no-photon exchange cross sections ($l = 0$) dominate throughout the energy range over the other two ($l = \pm 1$) for all values of $\mu$ except for $\mu = 0$where the single-photon absorption ($l = +1$) dominates.

Finally, we present some DCSs for both the singlet and triplet along with their corresponding FF results for $k_i = 0.5$ and $\mu = 0.02$. Strong modification is noted in the laser-assisted DCS as compared to the FF both quantitatively (suppression) and qualitatively for both the states with singlet all through lying slightly above the triplet. The oscillations noted in the LA DCS could be attributed to the oscillations of the Bessel functions occurring in the expression of DCS [vide Eq. (19)].

As may be noted from Figs. 7(a) and 7(b), at lower incident energies the FF TCS increases with increasing $\mu$. This may be physically attributed to the fact that for higher values of $\mu$, the effective size of the atom increases, thereby enhancing the cross sections, while at higher incident energy (beyond $k_i \sim 0.5$), the FF TCS becomes almost insensitive with respect to $\mu$ indicating that the effect of the Debye potential decreases with increasing incident electron energy.

## IV. CONCLUSIONS

The presence of the Debye-Hückel potential ($\mu > 0$) enhances the cross sections in all cases ($l = -1$, 0, and 1) and for all values of the incident momentum. Apart from the qualitative modifications, the major quantitative effect of the external laser field is to suppress the field-free cross sections. A significant difference is noted for the singlet and triplet cross sections. The suppression is much more in the triplet

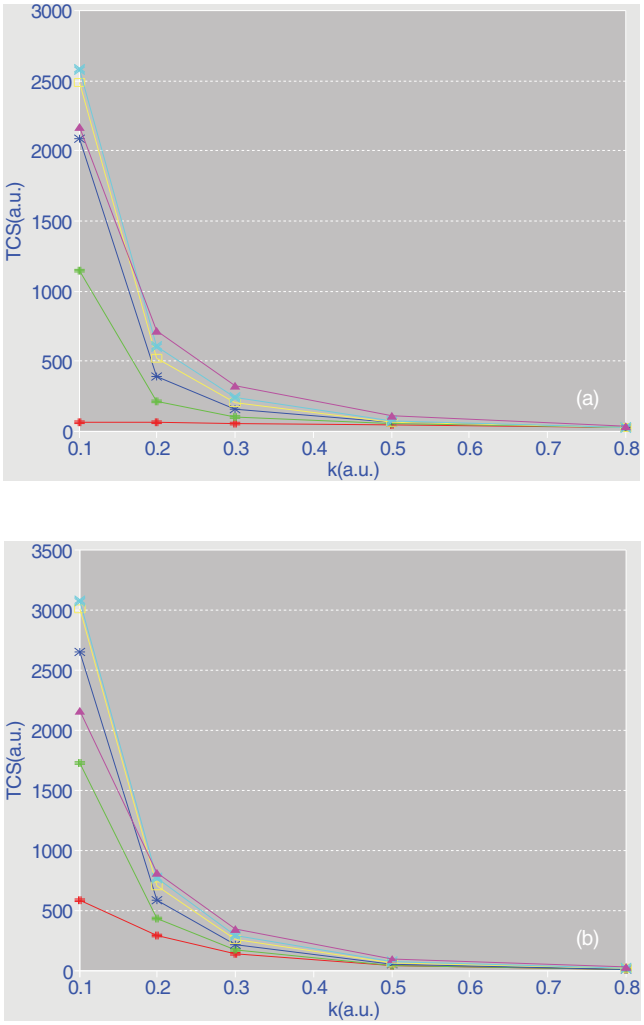


FIG. 7. (Color online) Total triplet (a) and singlet (b) FF cross sections (TCS) in a.u. against momentum $k_i$ (a.u.) for different values of $\mu$. The lowest curve is for $\mu = 0$ and the upper curves are for higher values of $\mu$ in increasing order, $\mu = 0.005$, 0.01, 0.015, 0.02, and 0.04.

states. Total cross sections decrease with the increase of the incident electron momentum and also with the increase of the Debye parameter, as expected. The DCSs exhibit a number of oscillations at lower scattering angles that could be attributed to the oscillations in the Bessel function.

## ACKNOWLEDGMENTS

Thanks are extended to the referee for helpful suggestions. Calculations were carried out using the Discovery Computer of the NASA Center for Computation Science.

## APPENDIX

The ground-state wave function of the target H atom gets dressed under the Debye-Hückel [22] potential and is given by

$$\phi_0 = e^{-ar} \sum_i C_i r^i. \tag{A1}$$

Since the lowest term does not contain $r$, the summation index ranges from 0 to $N = 14$, i.e., we have 15 terms in the expansion. The corresponding ground-state energy is calculated variationally by using

$$\langle \phi_0 | - \nabla_2^2 - \frac{2Z}{r_2} e^{-\mu r_2} | \phi_0 \rangle = E_0 \phi_0. \tag{A2}$$

In this Appendix, we give the ground-state energy of the hydrogen atom for various values of Debye parameter $\mu$ (vide Table I). We find that the energy is not sensitive to the variation of the parameter $a$ in the expansion given in Eq. (A1) and as such we kept it fixed at 1.0. The justification for this choice is provided by the energy values for a few parameters $a$: for $\mu = 0.0$ and $a = 0.90, 0.95, 0.97$, and 1.0, the ground-state energy is always equal to $-1.00$ Ry. For $\mu = 0.12$ and the same above values of $a$, the ground-state energy is $-0.7801$ Ry to four significant figures. The ground-state energies for various values of the Debye parameter $\mu$ are given in Table I. The results are accurate up to the figures quoted. As $\mu$ increases, the ground-state energy moves towards the continuum. Finally, for large values of $\mu$, the atom becomes unbound.

[1] S. Chakraborty and Y. K. Ho, Phys. Rev. A **77**, 014502 (2008).
[2] S. Paul and Y. K. Ho, Phys. Plasmas **17**, 082704 (2010).
[3] A. Ghoshal and Y. K. Ho, Eur. Phys. J. D **55**, 581 (2009).
[4] B. L. Whitten, N. F. Lane, and J. C. Weisheit, Phys. Rev A **29**, 945 (1984).
[5] R. S. Pundir and K. C. Mathur, J. Phys. B **17**, 4245 (1984).
[6] G. J. Hatton, N. F. Lane, and J. C. Weisheit, J. Phys. B **14**, 4879 (1981).
[7] B. N. Chichikov, J. Phys. B **23**, L103 (1990).
[8] A. Chattopadhyay and C. Sinha, J. Plasma Fusion Res. **7**, 286 (2006).
[9] Y. Chen, Phys. Rev. A **84**, 043423 (2011).
[10] M. B. S. Lima, C. A. S. Lima, and L. C. M. Miranda, Phys. Rev. A **19**, 1796 (1979).
[11] F. Brunel, Phys. Rev. Lett. **59**, 52 (1987).
[12] S. Alexiou, J. Quant. Spectrosc. Radiat. Transf. **71**, 139 (2001).
[13] S. Alexiou, P. Sauvan, A. Poquerusse, E. Leboucher-Dalimier, and R. W. Lee, Phys. Rev. E **59**, 3499 (1999).
[14] O. Blokhintsev, Phys. Z. Sowjetunion **4**, 601 (1933).
[15] *Methods of Experimental Physics*, Vol. 9, edited by H. R. Griem and R. H. Lovberg (Academic Press, New York, 1970), p. 115.
[16] A. Weingartshofer, J. K. Holmes, G. Caudle, E. M. Clarke, and H. Kruger, Phys. Rev. Lett. **39**, 269 (1977).
[17] A. Weingartshofer, E. M. Clarke, J. K. Holmes, and C. Jung, Phys. Rev. A **19**, 2371 (1979).
[18] N. J. Mason, Rep. Prog. Phys. **56**, 1275 (1993).
[19] B. Wallbank and J. K. Holmes, J. Phys. B **29**, 5881 (1996).

[20] M. O. Musa, A. McDonald, L. Tidswell, J. Holmes, and B. Wallbank, J. Phys. B **43**, 175201 (2010).
[21] C. Sinha and A. K. Bhatia, Phys. Rev. A **83**, 063417 (2011).
[22] P. Debye and E. Hückel, Phys. Z. **24**, 185 (1923).
[23] N. M. Kroll and K. M. Watson, Phys. Rev. A **8**, 804 (1973).
[24] A. Chattopadhyay and C. Sinha, J. Phys. B **37**, 3283 (2004).
[25] A. Chattopadhyay and C. Sinha, Phys. Rev. A **72**, 053406 (2005).
[26] G. N. Watson, *Theory of Bessel Functions*, 2nd ed. (Cambridge University Press, Cambridge, 1962), p. 22.
[27] A. K. Bhatia and A. Temkin, Phys. Rev. A **64**, 032709 (2001).
[28] K. Omidvar, Phys. Rev. **133**, A970 (1964).
[29] A. Temkin and J. C. Lamkin, Phys. Rev. **121**, 788 (1961).
[30] A. K. Bhatia, Phys. Rev. A **75**, 032713 (2007).